

# Single Event Effects in High-Energy Accelerators

Rubén García Alía<sup>1</sup>, Markus Brugger<sup>1</sup>, Salvatore Danzeca<sup>1</sup>,  
Francesco Cerutti<sup>1</sup>, Joao Pedro de Carvalho Saraiva<sup>1</sup>,  
Reiner Denz<sup>1</sup>, Alfredo Ferrari<sup>1</sup>, Lionel L. Foro<sup>1</sup>, Paul  
Peronnard<sup>1</sup>, Ketil Røed<sup>2</sup>, Raffaello Secondo<sup>1</sup>, Jens  
Steckert<sup>1</sup>, Yves Thurel<sup>1</sup>, Iacopo Toccafondo<sup>1</sup>, Sławosz  
Uznanski<sup>1</sup>

<sup>1</sup> CERN, CH-1211 Genve 23, Switzerland

<sup>2</sup> University of Oslo, Blindern NO-0316 Oslo, Norway

E-mail: ruben.garcia.alia@cern.ch

## Abstract.

The radiation environment encountered at high-energy hadron accelerators strongly differs from the environment relevant for space applications. The mixed-field expected at modern accelerators is composed of charged and neutral hadrons (protons, pions, kaons and neutrons), photons, electrons, positrons and muons, ranging from very low (thermal) energies up to the TeV range. This complex field, which is extensively simulated by Monte Carlo codes (e.g. FLUKA) is due to beam losses in the experimental areas, distributed along the machine (e.g. collimation points) and deriving from the interaction with the residual gas inside the beam pipe. The resulting intensity, energy distribution and proportion of the different particles largely depends on the distance and angle with respect to the interaction point as well as the amount of installed shielding material. Electronics operating in the vicinity of the accelerator will therefore be subject to both cumulative damage from radiation (Total Ionizing Dose, Displacement Damage) as well as Single Event Effects (SEEs) which can seriously compromise the operation of the machine. This combined with the extensive use of COTS (Commercial-Off-The-Shelf) components due to budget, performance and availability reasons, results in the need of carefully characterizing the response of the devices and systems to representative radiation conditions.

## 1. Introduction

Due to the rare nature of the reaction products that are of interest to high-energy particle physics, a vast quantity of interactions need to be generated to produce them. The number of interactions per unit surface and time is known as luminosity, and the performance of a collider can be qualified by its ability to deliver integrated luminosity. The latter can be enhanced by (i) increasing the luminosity (involving technological enhancements such as more powerful magnets or superconducting links) and/or (ii) by increasing the operational time, also referred to as availability [1]. As will be detailed below, radiation effects on electronic systems can significantly compromise the availability of a high-energy accelerator, and therefore improving the overall radiation hardness can have a very positive impact on increasing the operational time and in turn the delivered integrated luminosity. The typical unit of integrated luminosity is the inverse femtobarn ( $\text{fb}^{-1}$ , a unit proportional to the number of proton-proton interactions in the accelerator, and corresponding roughly to  $10^{14}$  collisions at TeV energies).

The availability of the Large Hadron Collider (LHC) machine is limited by its operation cycle. Protons needs to be injected and accelerated to their collision energy (nominally 7 TeV) in a process known as turnaround which during 2012 took in average 5.5 hours. After this time the beam is used for physics production in what is known as stable beam conditions. The duration of an uninterrupted stable beam cycle is roughly from 10 to 15 hours after which the beam is dumped due to its intensity loss in the collision points and other locations in the accelerator. During 2012 operation however, roughly 70% of the dumps were premature with an average stable beam duration of around 6 hours. 70 dumps out of a total of 409 were attributed to radiation effects, which when expressed in units of integrated luminosity correspond to roughly 3 radiation dumps per  $\text{fb}^{-1}$ . During 2015, the value was further decreased to  $\sim 2$  dumps per  $\text{fb}^{-1}$ . These figures represent a considerable improvement with respect to 2011 for which  $\sim 13$  dumps per  $\text{fb}^{-1}$  were attributed to radiation effects. This significant improvement was achieved in the scope of the Radiation to Electronics (R2E) project at CERN through short-term measures such as relocation, shielding reinforcement and (to a lesser extent) replacing sensitive equipment with more robust versions.

Ultimately, the goal for an acceptable High Luminosity LHC (HL-LHC, a machine upgrade to increase the integrated luminosity by a factor 10 planned for 2025 [2]) operation will be that less than 0.1 dumps per  $\text{fb}^{-1}$  are due to radiation. In order to achieve this, the mitigation techniques introduced above will clearly not suffice due to e.g limitations

such as the available space for extra shielding or maximum connection distance between the system and the accelerator. Therefore, for the mid and long-term, prevention will be more efficient than mitigation in terms of increasing the radiation reliability, the latter involving taking radiation hardness into account at a very early stage of the electronic system design and development.

In order to define the test requirements and estimate the impact of the sensitivity of a component or system, the knowledge of the associated radiation field is essential. As will be shown in Sections 2 and 3, the radiation environment in the LHC is typically calculated using the FLUKA Monte Carlo code [3–5] and monitored with the RadMON system [6, 7].

Furthermore, though also affected by cumulative radiation effects such as Total Ionizing Dose (TID) or Displacement Damage (DD), Single Event Effects (SEEs) are the dominating reliability threat to commercial electronics in the high-energy accelerator context. As will be detailed in Section 4, this is mainly due to the very large number of components and equipment installed. For cumulative effects and as long as the radiation levels are below the values that will significantly degrade the device's performance, increasing the number of parts or units will not result in an increased risk of failure due to radiation. Alternatively, whereas the SEE Mean-Time-Between-Failures (MTBF) for a single unit might be large enough not to negatively impact the accelerator operation, the increased number of units will have a direct impact on the failure rate. As will be discussed in Section 5 this also has implications on the associated test strategies. In addition, whereas measures such as rotating - e.g. alternating between locations with different radiation levels in an optimized manner - or replacing equipment are efficient in terms of reducing the impact from cumulative effects, due to their stochastic nature the sensitivity to SEEs cannot benefit from such solutions.

Moreover, whereas critical space applications or high-energy physics experiments typically rely on custom electronics that is radiation-hardened by design (RHBD) in the high-energy accelerator context, Commercial-Off-The-Shelf (COTS) components are the only possible solution due to cost, performance and availability constraints. The trade-off of benefiting from a state-of-the-art performance at a relatively low cost and with a high availability is of course that of having to qualify the candidate components against radiation and accepting or rejecting them according to their response.

no hay  
cita en  
donde se  
separan  
SEE  
de efectos  
cumulativos

Hadron  
Ozone  
nucl

## 2. Radiation Environment

### 2.1. High Energy Hadrons

In the high-energy accelerator context, SEEs are typically induced by indirect energy deposition events from nuclear interactions between the hadrons in the radiation environment and the nuclei in the component sensitive area. To this regard, the situation is similar to that encountered in the trapped proton belts or at ground level. Therefore, the SEE-relevant radiation environment is described through the so-called High Energy Hadron (HEH) fluence, defined as the time-integrated flux of hadrons above 20 MeV [8, 9]. The cutoff at 20 MeV applies to charged hadrons and is motivated by the associated energy loss in standard device packages coupled with rapidly decreasing nuclear reaction cross section below this energy, which renders charged particles below 20 MeV inefficient in terms of inducing SEEs. Under this hypothesis possible effects of direct ionization from singly charged particles [10] are therefore not taken into account and are considered in [11] from a Monte Carlo calculation perspective. In addition, in first approximation it is assumed that hadrons above 20 MeV are equally efficient in inducing SEEs owing to their similar interaction cross section and fragment properties in silicon [12, 13].

For neutrons, the significant energy loss through the package and nuclear reaction cross section decrease for energies below 20 MeV do not apply. Therefore, two further contributions need to be included in the SEE-relevant description of the environment. The first is related to neutrons in the 0.2 - 20 MeV range, which are capable of generating high-LET secondaries through elastic and inelastic interactions with nuclei in or near the Sensitive Volume (SV). In order to account for their contribution to the SEE rate and as will be detailed in Section 3, an empiric fit to the SEU cross section of a specific SRAM memory in the 5-15 MeV, supported by nuclear interaction cross section data, is used as a response function. When added to the HEH fluence, the total quantity is defined as HEH-equivalent fluence and therefore also includes the contribution from intermediate energy neutrons.

In addition, neutrons can also induce SEEs through capture reactions, notably at thermal energies. This is particularly relevant for components with a high  $^{10}\text{B}$  content near their sensitive region, owing to the large neutron capture cross section resulting in the emission of two energetic  $^4\text{He}$  and  $^7\text{Li}$  ions. In order to quantify their potential contribution to the high-energy accelerator SEE rate, the R-factor is defined as the ratio between the equivalent thermal neutron and HEH fluences[14], where the former is defined as the neutron flux weighted by the capture cross section in

$$R = \frac{\Phi_{\text{eq. Th. N}}}{\Phi_{\text{HEH}}} \quad (\Phi_{\text{eq. Th. N}})$$

$$\therefore \Phi_{\text{eq. Th. N}} = \sigma_{\text{capture cross}} \cdot \Phi_{\text{neutron flux}}$$

$^{10}\text{B}$  relative to the value at 0.025 eV. For the LHC shielded areas, the R-factor order of magnitude can be as large as  $10^2$ .

Finally, whereas the HEH fluence is useful in terms of quantifying the SEE risk, the Total Ionizing Dose (TID) and 1 MeV neutron-equivalent fluence (1 MeV  $\text{n}_{\text{eq}}$ ) are relevant in terms of quantifying cumulative damage effects. Though the ratio between the various quantities can vary significantly depending on the specific radiation environment, as a general approximation the estimation shown in Eq. 1 can be applied in the LHC context:

$$10^9 \text{ HEH/cm}^2 \sim 10^{10} \text{ 1MeV n}_{\text{eq}}/\text{cm}^2 \sim 1 \text{ Gy} \quad (1)$$

In Eq. 1 and throughout the paper, doses are referred to in Silicon.

### 2.2. Mixed-field sources and levels

Beam losses in high-energy accelerators can be divided into three categories according to their origin:

- (i) so-called "beam-cleaning" by collimator or collimator-like objects where part of the beam is intercepted in order to avoid distributed losses in other critical machine locations
- (ii) the particle collisions at experimental areas and the respective particle debris
- (iii) the interaction of the circulating beam with the residual gas inside the beam pipe (generally referred to as beam-gas)

Such beam losses lead to a very complex radiation field of mixed particle types and energies that will depend on (i) the accelerator operation conditions (ii) the distance and angle with respect to the interaction point and (iii) the amount of shielding (if any) between the interaction point and the concerned location.

In terms of layout [15], the LHC has eight arcs (ARC) and eight Long Straight Sections (LSS), the latter serving as experimental or utility insertions. In addition, 16 Dispersion Suppressors (DS) are located between the arcs and the LSS aiming at reducing the machine dispersion inside the insertions.

Areas exposed to radiation in the LHC context can be divided into two main categories: tunnel (in the ARC and DS) and shielded (in the LSS). The former, in which the amount of electronics is minimized, can be further categorized as the Dispersion Suppressor (DS, areas with higher radiation levels dominated by losses in the preceding Long Straight Sections, e.g. on collimators and absorbers) and ARC regions (dominated by beam-gas interactions). The shielded zones (also referred to as alcoves and hosting the majority of the accelerator's electronic equipment) can be further subdivided into heavily shielded areas close to the interaction points (and known as UJs)

and lightly shielded areas (known as RRs). Table 1 shows the expected annual HEH fluences and doses for nominal LHC conditions, defined as 7 TeV and  $50 \text{ fb}^{-1}/\text{yr}$ . For the HL-LHC ultimate luminosity ( $400 \text{ fb}^{-1}/\text{yr}$ ) these values are expected to increase by roughly a factor 10 - proportional to the luminosity scaling in first approximation.

**Table 1.** Expected worst-case annual radiation levels to electronics for nominal LHC operation conditions.

Area		$\Phi_{\text{HEH}} (\text{cm}^{-2}\text{yr}^{-1})$	TID ( $\text{Gy} \cdot \text{yr}^{-1}$ )
Tunnel	DS	$5 \cdot 10^9$	10
	ARC	$5 \cdot 10^8$	1
Alcoves	UJ	$1 \cdot 10^9$	1
	RR	$1.5 \cdot 10^8$	0.1

In order to compare these values with other reference environments, the annual HEH fluence at ground-level is  $\sim 2 \cdot 10^5 \text{ cm}^{-2}$  and  $\sim 3 \cdot 10^9 \text{ cm}^{-2}$  for a polar orbit of 800 km altitude and  $98^\circ$  inclination as calculated using CREME96 [16].

It is also worth noting that the values reported in Table 1 are relevant for locations that host electronic equipment in the LHC machine. In the LHC experiments however, the annual radiation levels to which the detector electronics will be exposed to after the HL-LHC upgrade are in the 1 MGy and  $10^{15} \text{ 1 MeV neq}$  order of magnitude [17, 18], which therefore typically require the use of electronics which is radiation hardened by design.

### 2.3. Radiation Environment Calculations

The complex high-energy accelerator field is simulated using the FLUKA Monte Carlo code [3–5]. FLUKA is a well benchmarked general purpose tool for the calculation of particle transport and interactions with matter, covering an extended range of applications such as electron and proton accelerator shielding, cosmic ray studies and medical physics.

With an adequate knowledge of the radiation source term and associated geometry, FLUKA can be used to calculate the radiation effects relevant quantities in the accelerator regions of interest and can therefore be used in the R2E context to predict the radiation levels for future machine conditions as well as to optimize solutions such as shielding or relocation. For instance, Fig. 1 shows a 2D horizontal cut of the expected HEH fluence for HL-LHC conditions near the ATLAS experiment in Point 1. As can be seen and despite the presence of the shielding, the expected HEH fluence levels in the UJ16 alcove region can be up to  $10^{10} \text{ cm}^{-2}\text{yr}^{-1}$ .

The FLUKA calculations of the radiation levels are also regularly benchmarked against measurements

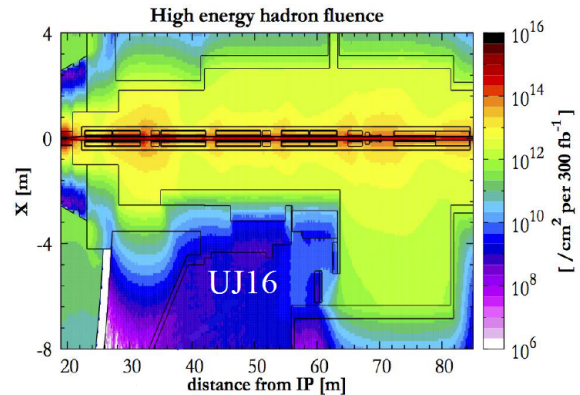


**Figure 1.** FLUKA HEH fluence for HL-LHC conditions around the triplet magnets and UJ16 area of Point 1.

with the monitors described in Section 3. This is done both for experimental facilities in which the high-energy accelerator environment is reproduced at larger rates and actual accelerator locations [8, 9, 12, 19].

Moreover, though this work focuses on the LHC environment, radiation effects in the LHC injector chain can also seriously compromise the overall performance of the machine. Therefore, a respective study of the radiation levels and corresponding benchmark with measured values is essential. As shown in [20, 21], the annual radiation levels reached in the LHC injectors such as the PS (accelerating protons up to 24 GeV) or SPS (reaching 450 GeV) can be larger than those in the LHC machine itself - experiments excluded.

In addition to the integrated levels, the energy spectra of mixed-field hadrons can be characterized using FLUKA and are also relevant to the SEE radiation hardness analysis. An example of the LHC tunnel hadron energy spectra can be seen in Fig. 2. As is observed, the hadron spectra extend up to energies well above the GeV range. This contrasts with the trapped proton radiation environment in which the spectrum falls off abruptly above 400 MeV [22]. As has been shown in [23–27], components with high-LET thresholds and high-Z materials near the SVs (e.g. tungsten in metalization layers and contacts) can have a very strong SEE cross section dependence with energy, therefore the hardness of the experimental and operational environments needs to be taken into account when performing SEE rate predictions, as will be further detailed in Section 5.

## 3. Monitoring Requirements and Solutions

### 3.1. Requirements and General Approach

An on-line monitoring system in the LHC tunnel and its adjacent areas is essential in order to provide a

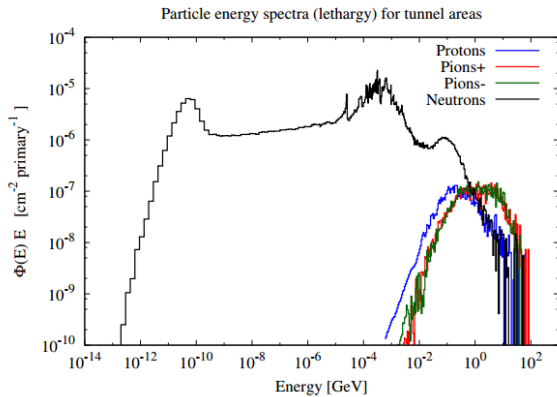


**Figure 2.** Simulated particle energy spectra representative for the tunnel areas in the LHC normalized to one proton-proton collision [9].

detailed knowledge of the associated radiation levels. This information has a very direct impact on the design, characterization and installation of electronic equipment as well as on possible relocation or shielding requirements.

Standard monitoring systems for accelerators are optimized to allow for proper beam steering and the detection of beam losses for machine protection purposes, and are not necessarily relevant in terms of describing the radiation levels and the associated radiation damage at the locations of the electronic equipment. For this reason, a dedicated RadMON system has been developed to cover this need [6, 7], allowing for the continuous monitoring of the three quantities important for radiation damage to electronics: high energy hadron fluence, total ionizing dose and 1 MeV neutron equivalent fluence. The RadMON system consists of a main board with an Actel ProAsic3 control FPGA and a 16-bit ADC for the readout of the analogue sensors, and a detector board hosting the SRAM banks and analogue sensors for TID and DD. The TID limit of the system is 200 Gy and is imposed by the ADC. However, a deported module is available for which the analogue sensors can be set up to 100m away from the main board, thus allowing the measurement of much larger dose levels.

The use of the detector is not limited to the LHC and its injectors but also covers the associated past and present CERN experimental areas such as H4IRRAD, CNRAD or CHARM. In addition, a cubesat version of the monitor is currently under development and will be flown in the CELESTA mission; a student satellite developed by CERN and the University of Montpellier.

As introduced in Section 2, the physical quantity relevant for SEE induction in the high-energy accelerator environment is the HEH fluence. Therefore, an LHC radiation detector must be able to measure this

value and thus also needs to have its response carefully calibrated against it. This procedure is highly challenging considering the mixed nature of the high-energy accelerator environment both in terms of SEE-relevant particle species and energies, and requires a combination of experimental and simulation efforts, as will be detailed below.

### 3.2. SRAM-based Detectors

SEUs are unwanted bit-flips in memory elements which can lead to data corruption or even system malfunction when occurring in configuration bits. However, their non-destructive nature can also be used as a means of characterizing radiation fields when appropriately calibrated.

The SEU response of commercial SRAM memories make them a convenient choice for measuring the SEE-relevant radiation environment in high-energy accelerators for various reasons, including their availability on the market, their representativeness of state-of-the-art CMOS technology radiation response, and their relatively low critical charge and therefore high sensitivity. Several requirements apply to SRAMs intended as SEU Monitors, such as being insensitive to destructive events such as SEL or having relatively high TID limits. In addition, the SEU sensitivity per device should be as large as possible, have a small spread amongst different individual components, and not depend on other environmental parameters such as TID or temperature. As will be detailed further on, it should also not be sensitive to other sources of SEUs such as bursts. Finally and in order to simplify the calibration process, it should as much as possible follow the HEH approximation, i.e. having a roughly constant SEU cross section above 20 MeV and not being sensitive to other particles such as e.g. thermal neutrons or direct ionization from singly charged particles. The potential contribution of particles or energies not considered in the HEH approach can then be derived using different operation conditions or complementary detectors.

In this section we present several different SRAM memories characterized for radiation detection purposes in the high-energy accelerator context. Due to the similarities outlined in Section 2, these detectors can also be used in other hadron environments such as the ground-level, avionic or trapped proton belt cases.

In the HEH approximation, the SEE response of an electronic component is assumed to be a step function with an onset at 20 MeV. Therefore, its HEH cross section can be evaluated at any given energy above this value. For LHC SRAM detectors this is typically carried out using the 200 MeV proton beam at PSI [28], where lower energies (typically down to 30 MeV) are also used by degrading the initial beam

in order to also evaluate the energy dependence of the response.

As SRAM detectors are typically distributed along the accelerator and can add up to several hundred units, it is not practical to perform individual cross section calibrations. For this reason, a statistically significant sample of devices coming from the same lot needs to be calibrated in order to retrieve not only an average cross section value but also an associated sensitivity spread. This is typically done for one specific energy and then applied to the overall interval of interest.

In addition and as detailed in [8], neutrons below 20 MeV can have a significant impact on the high-energy accelerator SEE rate. Moreover, their relative contribution will largely depend on the mixed-field composition and energy spectra, and can even play a dominating role for highly shielded regions such as the UJs. Therefore, it is important to characterize the response of SRAM detectors in this energy range. This is typically done at quasi-monoenergetic neutron facilities such as PTB in Braunschweig, Germany [29], where parts are tested at 5, 8 and 15 MeV. The respective relative cross section values can then be fitted to a Weibull curve which can in turn be used as an analytic response function.

An example of an SRAM detector calibration for high energy protons (30-230 MeV) and intermediate energy neutrons (5-15 MeV) is shown in Fig. 3 for the TC554001AF7L Toshiba SRAM used in the RadMON v5. Results are normalized to the highest energy point (230 MeV) for two different operation voltages which as will be detailed later are used to retrieve the equivalent thermal neutron fluence. The parameters of the Weibull fit of the response are also included. As can be seen, the SEU cross section is constant within  $\pm 20\%$  above 30 MeV and falls off rapidly with energy below that. Though very similar in relative terms, in absolute terms the 3V SEU cross section in the interval shown is a factor 2.3 larger than at 5V. For thermal neutrons, the respective ratio is 55.

The other two SRAM memories also calibrated and used for LHC and experimental area monitoring purposes (AT60142F 0.25  $\mu\text{m}$  ATTEL and Cypress 90 nm CY62157EV30) show normalized neutron and proton response functions which are qualitatively similar to that shown in Fig. 3 but which quantitatively can lead to different sensitivities in the mixed-field environment [30,31].

As for what regards the absolute value of the HEH cross section for the concerned memories, it is in the  $10^{-14}\text{cm}^2/\text{bit}$  order of magnitude for the Toshiba and ATTEL memories (4 Mbit), and  $10^{-13}\text{cm}^2/\text{bit}$  for the Cypress (8 Mbit).

Likewise, SEU detectors can be sensitive to

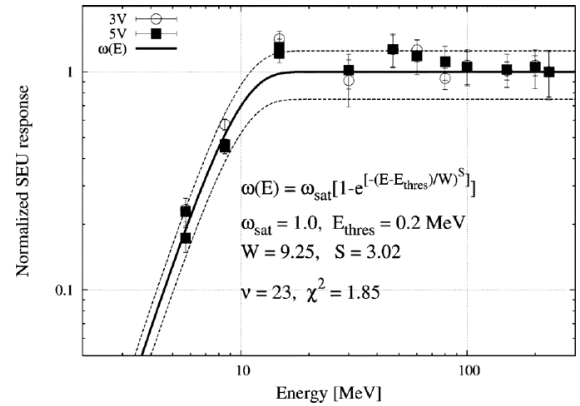


**Figure 3.** Normalized SEU response function for the TC554001AF7L Toshiba SRAM used in the RadMON v5 as shown in [9]. The three first points correspond to neutron measurements in the 5-15 MeV range whereas the rest are protons.

thermal neutrons. This is typically the case for feature sizes of 0.25  $\mu\text{m}$  and above, for which  $^{10}\text{B}$  had not yet been removed from the Boron Phosphor Silicate Glass (BPSG) [32]. The TC554001AF7L Toshiba SRAM used in the RadMON v5 is of the 0.4  $\mu\text{m}$  technology is very sensitive to thermal neutrons, especially when operated at 3V. By performing measurements at 3V and 5V for the same environment, the HEH and thermal neutron equivalent fluences can be retrieved as detailed in [14]. On the other hand, for most applications the Cypress 90 nm CY62157EV30 can be considered as insensitive to thermals, with a cross section two orders of magnitude lower than that for HEHs [7,30]. For the AT60142F ATTEL memory in the ESA SEU Monitor and with a feature size of 0.25  $\mu\text{m}$ , the thermal neutron cross section is one order of magnitude lower than the HEH one [33] and can therefore play an important role in the overall SEU rate for locations with large R-factors (i.e. thermal neutron to HEH fluence ratio as introduced above).

As mentioned above, one of the assumptions of the HEH formalisms is that hadrons above 20 MeV have a constant SEU cross section. As has been shown through mono-energetic measurements at TRIUMF (480 MeV), CHARM (24 GeV), CERF (120 GeV) or H4IRRAD (400 GeV) for the SEU detectors considered there is still a certain cross section increase above 200 MeV that is the energy typically used as representative of the HEH response. As detailed in [13] for the AT60142F ATTEL memory, this increase is expected to be due to the enhanced light fragment production in the device's overlayers (e.g. package or lid) for projectile energies in the 200 MeV - 3 GeV interval, which can lead to an SEU cross section increase of a factor 2-3. In addition, this trend is only observed when the part is tested with its 250  $\mu\text{m}$  Kovar

lid on, and is expected to be more pronounced for more integrated CMOS technologies. The respective impact can be carefully evaluated through tests at highly energetic mixed-field locations such as those available downstream the target at CHARM (as will be detailed in Section 5) as well as through Monte Carlo semi-empirical models calibrated to experimental results at lower energies. For silicon-dominated SEU cross sections, the impact of the cross section increase above 200 MeV in the mixed-field environment is only relevant for radiation environments with very hard energy spectra (e.g. the LHC tunnel).

As to what concerns the 90 nm Cypress memory, during its calibration sudden jumps of up to several thousand SEUs were observed without any apparent correlation with the beam conditions. These events are referred to as bursts and characterized by the fact that they affect memory cells sharing electrical contacts and thus following regular physical patterns. They are attributed to micro-latchups when the memory is operated in dynamic mode. As their occurrence depends on the operation condition and potentially also the specific radiation environment, burst can lead to wrong fluence measurement values. Based on their specific topology, in [34] an approach was introduced for the on-line detection and correction of the burst events through an FPGA-embedded algorithm. This solution has now been implemented in the v6 RadMONs and validated in the CHARM test facility.

### 3.3. Other Detectors

In addition to SEEs and as introduced in Section 1, TID is also a major concern for the reliability of electronics in high-energy accelerators. Therefore, monitoring this quantity is also of uttermost importance.

In the RadMON system, TID is measured with RadFETs, which are p-channel MOSFETs whose voltage threshold shift ( $\Delta V_{th}$ ) due to ionization in its gate oxide can be correlated with the TID that induces the effect. In the LHC context, RadFETs of three different oxide thicknesses (100, 400 and 1000 nm) have been calibrated in  $^{60}\text{Co}$  sources up to TID levels of roughly 10 kGy for the 100 nm case.

Though typically calibrated using a  $^{60}\text{Co}$  source, the RadFETs operate in high-energy accelerator environment for which depending on the exact locations, the contribution to the dose as calculated through FLUKA simulations is typically roughly evenly distributed among (i) photons (ii) electrons and positrons and (iii) charged hadrons and muons, with neutrons also potentially playing an important role for highly shielded locations. As confirmed through mono-energetic radiation testing, the  $\Delta V_{th}$  induced for a given deposited dose can vary depending on the

particle species and energy. For instance, protons of 30 MeV were shown to induce a reduced  $\Delta V_{th}$  when compared to higher energy protons or photons. This is attributed to the fact that, owing to the larger ionization density, the columnar recombination process dominates rendering the charge collection less efficient. However and as quantified in [35] the  $^{60}\text{Co}$  calibration for a relatively thin oxide (100 nm) can be applied to a high-energy accelerator mixed-field with an associated uncertainty of  $\pm 25\%$ .

As a complementary solution to the RadFET, a floating-gate dosimeter (FGDOS) has been studied [36]. In the FGDOS several radiation-induced mechanisms lead to the discharging of the gate, thus inducing a variation in the gate potential which can therefore be correlated to the associated TID level. One of the main possible advantages of the FGDOS detector is that it can reach a dose resolution of 0.3 mGy(Si) which corresponds to roughly a factor 200 improvement with respect to the 60 mGy(Si) achievable with the 100 nm RadFET biased at 5V. In addition, the FGDOS is built on a standard CMOS process and unlike the RadFET does not require a custom process to grow a thick oxide. Moreover, the FGDOS can be charged back to its initial state, essentially making it re-usable. In terms of the associated calibration challenges and in addition to those related to the response dependence on TID and particle type and energy (already introduced for the RadFET) the FGDOS also showed a relatively strong dependence on the dose rate and a TID life-time of roughly 200 Gy which can in principle be increased through mitigation techniques at ASIC design level.

Another very attractive radiation level monitoring system recently developed in the LHC and injector context is the Distributed Optical Fiber Radiation Sensor (DOFRS) based on Radiation Induced Attenuation (RIA). The main advantage of DOFRS is that, as opposed to punctual radiation level measurements such as those provided by the RadMON, the dose can be measured in a distributed way, with a meter-scale spatial resolution. Indeed, this is an extremely attractive property for a 27 km accelerator such as the LHC. In the scope of the R2E project, Phosphorous co-doped fibers selected due to their relatively independent response to dose rate were tested using both  $^{60}\text{Co}$  and the mixed-field at CHARM [37]. The fibers provide a linear response up to several tens of kGy and can offer a different dose resolution and dynamic range depending on their exact composition and the optical wavelength with which they are interrogated.

#### 4. Applications, Large Systems and Dependency on COTS

Cabling and distance constraints imply that certain LHC systems such as the power converters providing up to 13 kA current to the superconducting magnets, the pumps needed to create the vacuum conditions required in the beam pipe or the cryogenic system used to reach the temperature of 4K, are installed near the actual accelerator and therefore exposed to high radiation levels. Moreover, provided that systems can be replicated up to over 1000 times along the accelerator, each hosting up to several tens of different electronic components, the use of radiation hardened by design solutions at a component level is often not possible due to budget constraints as well as sometimes electrical performance requirements. Therefore, equipment systems in the LHC are either fully commercial, or at least based on COTS components.

However, in order to use reliable COTS-based systems in the high-energy accelerator environment, a failure analysis needs to be performed based on the expected radiation levels and qualified response of the component. To this regard, the degradation of the performance of a component due to TID or DD might be acceptable as long as it does not compromise the system in which it is embedded, and a certain SEE sensitivity can be tolerated if it is expected to cause only an acceptable number of stops in the accelerator. In a global sense, the overall SEE failure cross section for the nominal LHC conditions (peak luminosity of  $10^{34} \text{ cm}^{-2} \text{s}^{-1}$  and yearly integrated luminosity of  $50 \text{ fb}^{-1}$ ) is 0.5 dumps per  $\text{fb}^{-1}$ , which corresponds to a MTBF of roughly 2 weeks. In addition to this overall consideration, failures also need to be weighted by their impact on the operation of the machine, which can range from being transparent and only involving the loss of monitoring data, through not leading to a dump but requiring an access in the next possible intervention slot, to directly leading to a dump and potentially also requiring an intervention.

As an example of the failure analysis approach, we consider the FGCLite system [38], which is a controller for the LHC power controllers consisting of high-precision digital and analogue electronics. Due to these high-precision requirements, the FGCLite system is placed in the same rack as the power converter unit itself, directly adjacent to the LHC magnets. The radiation requirements of the FGCLite system are that of leading to less than 10 beam dumps per year for the nominal LHC operation scenario. Considering the individual locations of the more than 1000 units installed (with roughly 750 of them hosted in the LHC tunnel) and their respective expected HEH fluence levels, this would require a cross section lower than

$3 \cdot 10^{-12} \text{ cm}^2/\text{unit}$  [38]. In order to determine individual component cross sections in that order (or alternatively establish relevant upper limits) proton fluences of  $\sim 10^{13} \text{ cm}^{-2}$  would need to be reached, involving roughly 13 hours of beam time per component at PSI and dose levels of roughly 6 kGy, potentially inducing other damage not relevant to the operational scenario where the individual levels would be much smaller, and thus not allowing to reach the targeted value on a single component.

An additional difficulty related to COTS component testing is the potential sensitivity difference from parts coming from different batches or lots. Typically component batches of several thousand units are procured, ideally all coming from the same fabrication lot, but this is not always possible. As an example, Fig. 4 shows the SEL proton cross section for different lots (i.e. date-codes, DC) of the K6R4016V1D-TC10 SRAM as tested by the European Space Agency (ESA) for benchmark with the Proba-II GPS Phoenix SEL rate [39, 40]. The part is also used in one of the LHC systems, namely the control board of the BTV/MTV used for beam observation, emittance measurements and initial beam steering [41]. As can be seen, depending on the DC and respective HEH cross section considered, the resulting estimated SEL rate in the failure analysis for an LHC environment varies by two orders of magnitude.

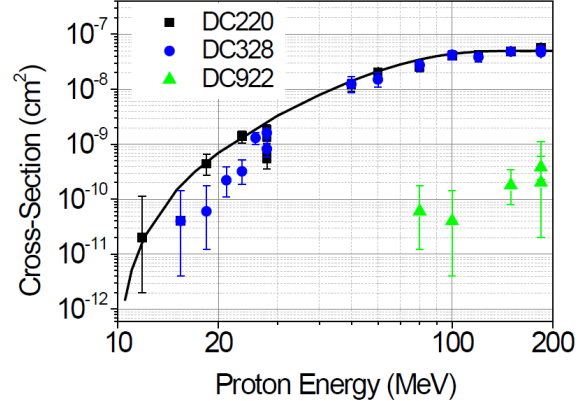


**Figure 4.** SEL cross section for different date-codes of the K6R4016V1D-TC10 SRAM as measured by ESA [40].

Finally, as it is not possible to fully characterize every single component in a system, priority levels need to be established according to (i) the impact of a potential failure at system level (ii) the available knowledge on the general response of the type of component and (iii) the availability of alternative components with equally valid electrical properties on the market. The associated component classification and resulting test methodology are summarized in Table 2.

**Table 2.** Component classification and respective test methodology.

Class	Radiation response	Sourcing	Test Methodology
Class-0 (potentially sensitive)	Resistant or moderately sensitive	Easily replaceable, different manufacturers available	Selection of already tested component when possible. Only integrated in system test.
Class-1 (potentially critical)	Potentially susceptible to radiation, not in system's critical path	Substitution possible (list of preferable replacements defined)	Sensitivity screening, if possible of several candidates. If passed, integrated in system test.
Class-2 (highly critical)	Potentially susceptible to radiation, on system's critical path	Difficult to replace, no equivalents on the market	Sensitivity screening and if passed, lot/batch testing. If accepted, integrated in system test.

In addition to the component types presently used in the high-energy accelerator context, emerging technologies in the rapidly evolving semiconductor industry offer attractive solutions but will need to be carefully characterized in the associated environment. For instance, wide bandgap power MOSFETs (e.g. SiC MOSFETs) will be used as solid-state switches in future beam extraction systems owing to their fast rise and fall times, high voltage and current ratings and low on-state resistance [42]. Whereas such components have shown to be more tolerant to TID than their silicon counterparts, their SEE sensitivity appears to be larger, with effects that still need to be interpreted [43, 44]. Likewise, the impact singly charged particle direct ionization [45, 46] or thermal neutrons [47, 48] in deep sub-micron technologies also needs to be evaluated as it concerns components which are very attractive in terms of processing capability (e.g. SRAM-based FPGAs) but for which the accelerator environment can have an impact very different to that in space or at ground level (e.g. large thermal neutron and muon fluxes in heavily shielded areas).

## 5. Radiation Hardness Assurance

### 5.1. Challenges and Strategy

As discussed in Section 4, the extensive use of COTS components and systems in the high-energy accelerator context requires a strategy to assure the reliability of the equipment in the defined radiation environment in order to permit for a safe and effective operation of the LHC machine. Therefore, one of the key points of the LHC Radiation Hardness Assurance (RHA) is that of defining the radiation environment relevant to the concerned system. To this regard, two major areas can be defined: the LHC tunnel, for which both stochastic (i.e. SEE) and cumulative (i.e. TID and DD effects) are relevant; and shielded areas, where only SEEs are to be considered.

Another important high-level distinction to be made when defining the RHA strategy is that of the type of system. In this sense, one can distinguish between (i) COTS systems and (ii) custom systems

based on COTS components. The former are fully commercial devices for which there is no control over the single components whose reference might even change from one system to the next. These type of systems should only be installed in the LHC shielded areas and can only be tested in the CERN test areas where large volumes can be placed. Although the system is a *black box* for the equipment engineer, its current consumption can be monitored in the accessible analogue test points, and interruptions in its operation or destructive effects can be identified and used to calculate the MTBF. Should the latter not comply with the radiation tolerance requirements for the system, mitigation techniques at system level such as the implementation of automatic resets, software fault diagnostics or the use of redundant subsystems need to be put in place.

Custom systems based on COTS components are designed by CERN engineers and can therefore be tested on a discrete component basis. When possible, components which have already been qualified are used. Otherwise, the strategy is to choose a set of references that comply with the electrical requirements of the system, purchase a few samples and pre-screen them. The selected component reference can then be purchased in a large quantity and tested by lot, leading to the acceptance or rejection of the lot. In the case of pre-tested components, the screening is no longer required, however a radiation test by lot will still be necessary. The general RHA guidelines for a high-energy accelerator COTS-based system are shown in Fig. 5 where the radiation-specific steps are marked in blue.

Based on the requirements, two partially complementary test approaches can be adopted. The first one consists in selecting and using external test facilities recognized by the radiation community. In the case of CERN, PSI is the standard facility for SEE (and partially TID) testing, CEA provides a neutron environment at  $\sim 1$  MeV for DD characterization, and the Fraunhofer institute is used for TID characterization using a  $^{60}\text{Co}$  source. The second strategy aims at using internal test facilities capable of directly reproducing a

radiation environment representative of that found in the accelerator. This approach is further developed in the following subsection.

### 5.2. The CHARM Test Facility

As a complementary approach to using external monoenergetic test facilities such as PSI or PTB, the high-energy accelerator mixed-field can be reproduced through the interaction of a high energy proton beam with a metallic target. In the past this was the approach followed at test areas such as H4IRRAD [49]. However, such areas were only operative a few weeks per year and were parasitic to other experiments, limiting their use for radiation effects testing. In order to improve this situation, the CHARM facility was built in the PS East Area at CERN and has been operating since late 2014 [19].

A sketch of the facility can be seen in the horizontal cut in Fig. 6. The 24 GeV beam extracted from the Proton Synchrotron (PS, one of the LHC pre-injectors) interacts with a 50 cm copper target generating a mixed-radiation field composed mainly of neutrons, pions and protons as to what concerns SEE-relevant particles. Other particles such as electrons/positrons, muons or photons are also present in the mixed-field in large proportions and contribute to the TID. The intensity and composition of the resulting radiation field largely depends on the test position and movable shielding configuration. Depending on the intended operational environment, a combination suitable for the LHC tunnel or shielded areas can be found. In addition, other radiation environments of interest such as the ground-level or trapped proton belt can also be reproduced. The radiation levels and particle energy spectra in the CHARM facility are simulated using the FLUKA Monte Carlo tool and benchmarked against

measurements with calibrated detectors such as the RadMON system introduced in Section 3.

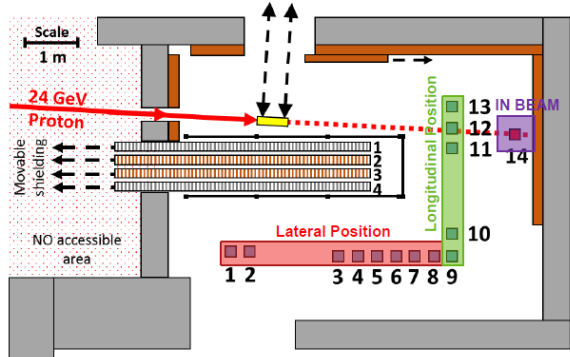


**Figure 6.** Horizontal cut of the CHARM radiation facility, with the PS beam entering from left to right and impinging on the copper target to generate the high-energy accelerator mixed-field.

Depending on the exact location and operation of the PS beam impinging on the copper target, the radiation level at CHARM for the lateral positions (see Fig. 6) and the copper target, no shielding configuration is  $\sim 2 \cdot 10^9$  HEH/h and  $\sim 1$  Gy/h. In the longitudinal test locations, such levels are roughly a factor 5 larger. When compared with Table 1 it can therefore be seen that typical annual HEH fluxes in the LHC accelerator can be reached at CHARM in just several hours of test time. In addition, the particle energy spectra encountered in the LHC tunnel and shielded areas can be closely reproduced, having an important impact on the SEE rate for cross sections dominated by high-Z materials and thus minimizing the risk of underestimating the failure rate due to testing with an insufficient monoenergetic energy or an excessively soft spectrum [27].

An important characteristic of the CHARM

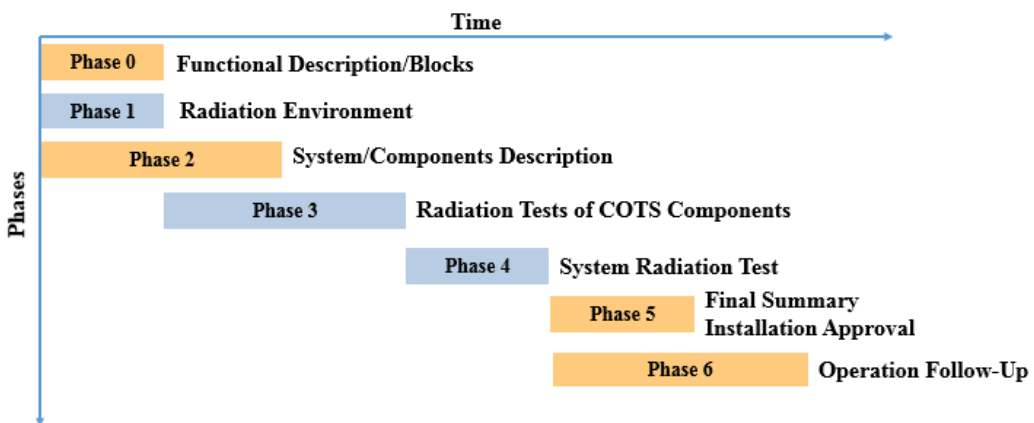


**Figure 5.** RHA assurance guidelines for COTS-based systems in the high-energy accelerator environment.

facility is that, as opposed to standard facilities in which collimated beams of several cm in diameter are used, the mixed-field fills the full irradiation chamber. This can pose constraints on the test setup, as the cable distance from the test positions to the radiation-free area (e.g. control room) is roughly 30m. However, it also enables the test of full systems [50] (e.g. LHC power converter, cubesat, etc.) or boards hosting tens or hundreds of components for batch testing. As discussed in Section 4, the system and batch testing aspects are essential for the high-energy accelerator radiation hardness assurance due to the very large number of components and systems involved.

In addition to CHARM, other complementary test facilities exist at CERN such as the 10 TBq  $^{60}\text{Co}$  source or a 200 MeV electron beam line for radiation effects testing known as VESPER [51].

## 6. Conclusions

The high-energy accelerator radiation field is of a complex nature which differs to that encountered at ground level or in space. The broad variety of particle species and their very large energy interval, ranging from thermal to TeV, makes it a very challenging radiation context which therefore needs to be calculated with Monte Carlo tools such as FLUKA and monitored with dedicated detectors such as the RadMON.

Whereas cumulative effects can have a negative impact on the performance of devices installed in the LHC tunnel, SEEs are typically the major source of concern in terms of radiation effects, especially in the shielded areas. This is partially due to the stochastic nature of SEEs and the very large number of system units the accelerator hosts. Due to this distributed nature, COTS components or systems are the baseline solution, thus requiring a characterization of their radiation response. The latter is performed according to the radiation levels in which the components will operate as well as to their criticality and availability of alternative options.

In addition to discrete component testing, full system tests need to be performed in order to validate the equipment as a whole. In the case of COTS systems, this is the only possible validation. For such characterization approach, the CHARM test facility is particularly attractive as (i) it reproduces a radiation environment very similar to that encountered in the high-energy accelerator context and (ii) its large radiation area can host full systems exposing them to a highly homogeneous radiation field.

## References

- [1] Apollonio A, Jonker M, Schmidt R, Todd B, Wagner S, Wollmann D, Zerlauth M *et al.* 2013 *TUPFI012, proceedings of IPAC 13*
- [2] Apollinari G, Bjar Alonso I, Brning O, Lamont M and Rossi L 2015 *High-Luminosity Large Hadron Collider (HL-LHC): Preliminary Design Report* (Geneva: CERN) URL <https://cds.cern.ch/record/2116337>
- [3] Ferrari A, Sala P R, Fasso A and Ranft J 2005 *CERN-2005-10-2005, INFN/TC-05/11, SLAC-R-773*
- [4] Böhnen T, Cerutti F, Chin M, Fassò A, Ferrari A, Ortega P, Mairani A, Sala P, Smirnov G and Vlachoudis V 2014 *Nuclear Data Sheets* **120** 211–214
- [5] 2015 *Annals of Nuclear Energy* **82** 10 – 18
- [6] Spiezzi G, Mekki J, Brugger M, Calviani M, Ferrari A, Kramer D, Losito R, Masi A, Nyul A, Peronnard P, Pignard C, Roed K and Wijnands T 2011 *Paper accepted by the Journal of Proceedings of Science* <http://pos.sissa.it/>. **58** 1001 –1007 ISSN 0018-9499
- [7] Spiezzi G, Peronnard P, Masi A, Brugger M, Brucoli M, Danzeca S, Alia R G, Losito R, Mekki J, Oser P, Gaillard R and Dusseau L 2014 *IEEE Trans. Nucl. Sci.* **61** 3424–3431 ISSN 0018-9499
- [8] Roed K, Boccone V, Brugger M, Ferrari A, Kramer D, Lebbos E, Losito R, Mereghetti A, Spiezzi G and Versaci R 2011 *IEEE Trans. Nucl. Sci.* **58** 932 –938 ISSN 0018-9499
- [9] Roed K, Brugger M, Kramer D, Peronnard P, Pignard C, Spiezzi G and Thornton A 2012 *IEEE Trans. Nucl. Sci.* **59** 1040 –1047 ISSN 0018-9499
- [10] Sierawski B D, Pellish J A, Reed R A, Schrimpf R D, Warren K M, Weller R A, Mendenhall M H, Black J D, Tipton A D, Xapsos M A, Baumann R C, Deng X, Campola M J, Friendlich M R, Kim H S, Phan A M and Seidleck C M 2009 *IEEE Trans. Nucl. Sci.* **56** 3085–3092 ISSN 0018-9499
- [11] Infantino A, Alia R G and Brugger M 2016 *IEEE Transactions on Nuclear Science* **PP** 1–1 ISSN 0018-9499
- [12] Alia R G, Biskup B, Brugger M, Calviani M, Poivey C, Roed K, Saigne F, Spiezzi G and Wrobel F 2013 *IEEE Trans. Nucl. Sci.* **60** 2469–2476 ISSN 0018-9499
- [13] Alia R G, Brugger M, Danzeca S, Ferlet-Cavrois V, Poivey C, Roed K, Saigne F, Spiezzi G, Uznanski S and Wrobel F 2013 *IEEE Trans. Nucl. Sci.* **60** 4142–4149 ISSN 0018-9499
- [14] Kramer D, Brugger M, Klupak V, Pignard C, Roed K, Spiezzi G, Viererbl L and Wijnands T 2011 *IEEE Trans. Nucl. Sci.* **58** 1117 –1122 ISSN 0018-9499
- [15] Evans L and Bryant P 2008 *Journal of Instrumentation* **3** S08001 URL <http://stacks.iop.org/1748-0221/3/i=08/a=S08001>
- [16] Tylka A J, Adams J H, Boberg P R, Brownstein B, Dietrich W F, Flueckiger E O, Petersen E L, Shea M A, Smart D F and Smith E C 1997 *IEEE Trans. Nucl. Sci.* **44** 2150–2160 ISSN 0018-9499
- [17] ATLAS C 2012 Letter of Intent for the Phase-II Upgrade of the ATLAS Experiment Tech. Rep. CERN-LHCC-2012-022. LHCC-I-023 CERN Geneva draft version for comments URL <https://cds.cern.ch/record/1502664>
- [18] Contardo D, Klute M, Mans J, Silvestris L and Butler J 2015 Technical Proposal for the Phase-II Upgrade of the CMS Detector Tech. Rep. CERN-LHCC-2015-010. LHCC-P-008. CMS-TDR-15-02 CERN Geneva. Geneva upgrade Project Leader Deputies: Lucia Silvestris (INFN-Bari), Jeremy Mans (University of Minnesota) Additional contacts: Lucia.Silvestris@cern.ch, Jeremy.Mans@cern.ch URL <https://cds.cern.ch/record/2020886>

- [19] Mekki J, Brugger M, Alia R, Thornton A, Dos Santos Mota N and Danzeca S 2015 A mixed field facility at CERN for radiation test: CHARM *Radiation and Its Effects on Components and Systems (RADECS)*, 2015 15th European Conference on pp 1–4
- [20] De Carvalho Saraiva J P and Brugger M 2015 URL <https://cds.cern.ch/record/2114889>
- [21] De Carvalho Saraiva J P and Brugger M 2015 Monte Carlo simulations and benchmark studies at CERN's accelerator chain Tech. rep.
- [22] Barth J L, Dyer C S and Stassinopoulos E G 2003 *IEEE Trans. Nucl. Sci.* **50** 466–482 ISSN 0018-9499
- [23] Schwank J R, Shaneyfelt M R, Baggio J, Dodd P E, Felix J A, Ferlet-Cavrois V, Paillet P, Lambert D, Sexton F W, Hash G L and Blackmore E W 2005 *IEEE Trans. Nucl. Sci.* **52** 2622 – 2629 ISSN 0018-9499
- [24] Alia R G, Brugger M, Danzeca S, Ferlet-Cavrois V, Poivey C, Roed K, Saigne F, Spiezzi G, Uznanski S and Saigne F 2014 *IEEE Trans. Nucl. Sci.* **61** 2718–2726 ISSN 0018-9499
- [25] Alia R G, Blackmore E W, Brugger M, Danzeca S, Ferlet-Cavrois V, Gaillard R, Mekki J, Poivey C, Roed K, Saigne F, Spiezzi G, Trinczek M, Uznanski S and Wrobel F 2014 *IEEE Trans. Nucl. Sci.* **61** 2936–2944 ISSN 0018-9499
- [26] Uznanski S, Alia R G, Blackmore E, Brugger M, Gaillard R, Mekki J, Todd B, Trinczek M and Villanueva A 2014 *IEEE Trans. Nucl. Sci.* **61** 3074–3079 ISSN 0018-9499
- [27] Alia R, Brugger M, Danzeca S, Ferlet-Cavrois V, Frost C, Gaillard R, Mekki J, Saigne F, Thornton A, Uznanski S and Wrobel F 2015 *IEEE Trans. Nucl. Sci.* **62** 2555–2562 ISSN 0018-9499
- [28] Hajdas W, Burri F, Eggel C, Harboe-Sorensen R and de Marino R 2002 Radiation effects testing facilities in PSI during implementation of the Proscan project *Radiation Effects Data Workshop, 2002 IEEE* pp 160 – 164
- [29] The PTB neutron reference fields (PIAF)-quasi-monoenergetic neutron reference fields in the energy range from thermal to 200 MeV
- [30] Danzeca S, Spiezzi G, Brugger M, Dusseau L, Foucard G, Alia R G, Mala P, Masi A, Peronnard P, Soltes J, Thornton A and Viererbl L 2014 *IEEE Trans. Nucl. Sci.* **61** 3458–3465 ISSN 0018-9499
- [31] Alia R G 2013 *Radiation Fields in High Energy Accelerators and their impact on Single Event Effects* Ph.D. thesis Universite Montpellier 2 URL <http://cds.cern.ch/record/2012360>
- [32] Baumann R C and Smith E B 2000 Neutron-induced boron fission as a major source of soft errors in deep submicron sram devices *Reliability Physics Symposium, 2000. Proceedings. 38th Annual 2000 IEEE International* pp 152–157
- [33] Harboe-Sorensen R, Poivey C, Guerre F X, Roseng A, Lochon F, Berger G, Hajdas W, Virtanen A, Kettunen H and Duzellier S 2008 *IEEE Trans. Nucl. Sci.* **55** 3082 –3087 ISSN 0018-9499
- [34] Secondo R, Foucard G, Danzeca S, Losito R, Peronnard P, Masi A, Brugger M and Dusseau L 2016 *IEEE Trans. Nucl. Sci.* **PP** 1–8 ISSN 0018-9499
- [35] Mekki J, Brugger M, Danzeca S, Dusseau L, Red K and Spiezzi G 2013 *IEEE Trans. Nucl. Sci.* **60** 2435–2443 ISSN 0018-9499
- [36] Danzeca S, Cesari J, Brugger M, Dusseau L, Masi A, Pineda A and Spiezzi G 2014 *IEEE Trans. Nucl. Sci.* **61** 3451–3457 ISSN 0018-9499
- [37] Toccafondo I, Thornton A, Guillerman E, Kuhnhenn J, Mekki J, Brugger M and Pasquale F D 2015 Distributed optical fiber radiation sensing at CERN high energy accelerator mixed field facility (CHARM) 2015 15th European Conference on Radiation and Its Effects on Components and Systems (RADECS) pp 1–4
- [38] Uznanski S, Todd B, Dinis A, King Q and Brugger M 2014 *IEEE Trans. Nucl. Sci.* **61** 3694–3700 ISSN 0018-9499
- [39] D'Alessio M, Poivey C, Ferlet-Cavrois V, Evans H, Harboe-Sorensen R, Keating A, Lopez-Calle I, Guerre F, Lochon F, Santandrea S, Zadeh A, Muschitiello M, Markgraf M, Montenbruck O, Grillenberger A, Fleurinck N, Puimege K, Gerrits D and Matthijs P 2013 SRAMs SEL and SEU in-flight data from PROBA-II spacecraft *Radiation and Its Effects on Components and Systems (RADECS), 2013 14th European Conference on* pp 1–8
- [40] Ferlet-Cavrois V, Muschitiello M and D'Alessio M 2013 *European Space Components Information Exchange System, ESCIES, Radiation database*
- [41] Bravin E, Ferioli G, MacCaferri R, Burger S, Focker G and Guerrero A 2005 A new TV beam observation system for CERN
- [42] Kramer T, Barna D, Barnes M, Bartmann W, Burkart F, Ducimetière L, Goddard B, Senaj V, Stadlbauer T and Woog D 2016 Considerations for the injection and extraction kicker systems of a 100 tev centre-of-mass fcc-hh collider *7th International Particle Accelerator Conference (IPAC'16), Busan, Korea, May 8-13, 2016* (JACOW, Geneva, Switzerland) pp 3901–3904
- [43] Mizuta E, Kuboyama S, Abe H, Iwata Y and Tamura T 2014 *IEEE Trans. Nucl. Sci.* **61** 1924–1928 ISSN 0018-9499
- [44] Shoji T, Nishida S, Hamada K and Tadano H 2015 *Microelectronics Reliability* **55** 1517–1521
- [45] Sierawski B, Mendenhall M, Reed R, Clemens M, Weller R, Schrimpf R, Blackmore E W, Trinczek M, Hitti B, Pellish J, Baumann R, Wen S J, Wong R and Tam N 2010 *IEEE Trans. Nucl. Sci.* **57** 3273–3278 ISSN 0018-9499
- [46] Dodds N A, Martinez M J, Dodd P E, Shaneyfelt M R, Sexton F W, Black J D, Lee D S, Swanson S E, Bhuva B L, Warren K M, Reed R A, Tripple J, Sierawski B D, Weller R A, Mahatme N, Gaspard N J, Assis T, Austin R, Weeden-Wright S L, Massengill L W, Swift G, Wirthlin M, Cannon M, Liu R, Chen L, Kelly A T, Marshall P W, Trinczek M, Blackmore E W, Wen S J, Wong R, Narasimham B, Pellish J A and Puchner H 2015 *IEEE Trans. Nucl. Sci.* **62** 2440–2451 ISSN 0018-9499
- [47] Autran J L, Serre S, Semikh S, Munteanu D, Gasior G and Roche P 2012 *IEEE Trans. Nucl. Sci.* **59** 2658–2665 ISSN 0018-9499
- [48] Yamazaki T, Kato T, Uemura T, Matsuyama H, Tada Y, Yamazaki K, Soeda T, Miyajima T and Kataoka Y 2015 *Journal of Vacuum Science Technology B* **33** 020604
- [49] Biskup B, Brugger M, Calviani M, Ethymiopoulos I and Kwee R 2014 *in Progress in Nuclear Science and Technology*
- [50] Casas-Cubillos J, Trikoupis N and Mekki J 2016 *IEEE Trans. Nucl. Sci.* **PP** 1–1 ISSN 0018-9499
- [51] Tali M, Alia R G, Brugger M, Ferlet-Cavrois V, Corsini R, Farabolini W, Santin G and Virtanen A *IEEE TNS, submitted for publication*